Remote Sensing of Environment 114 (2010) 761–771

Contents lists available at ScienceDirect

Remote Sensing of Environment

journal homepage: www.elsevier.com/locate/rse

Quantifying the spatial distribution of soil mass wasting processes after the 2008 earthquake in Wenchuan, China
A case study of the Longmenshan area

Baofeng Di [a,c,*], Hongjuan Zeng [b], Minghua Zhang [c], Susan L. Ustin [c], Ya Tang [a], Zhaoyin Wang [d], Ningsheng Chen [e], Bin Zhang [f]

[a] Department of Architecture & Environment, Sichuan University, Chengdu 610065, China
[b] School of Geography, Beijing Normal University, Beijing 100875, China
[c] Department of Land, Air, and Water Resources, University of California Davis, CA 95616, USA
[d] State Key Lab of Hydroscience and Engineering, Tsinghua University, Beijing 100084, China
[e] Chengdu Institute of Mountain Hazards and Environment, CAS, Chengdu 610041, China
[f] Land and Resources College, China West Normal University, Nanchong 637002, China

ARTICLE INFO

Article history:
Received 31 March 2009
Received in revised form 18 November 2009
Accepted 21 November 2009

Keywords:
Wenchuan Earthquake
Longmenshan scenic area (LMSS)
Mass wasting of soil
Landslides
RS
GIS

ABSTRACT

The beautiful Longmenshan area is one of the main tourist attractions in Sichuan Province, China. The epicenter of a catastrophic earthquake measured at 8.0 Ms (China Seismological Bureau), occurred within this area at Wenchuan (31°01′16″N, 103°22′01″E) at 14:28 May 12, 2008 (Beijing time). The earthquake triggered numerous types of landslide transport and hazards, including soil and debris avalanches, rockfalls, slumps, debris flows, creation of barrier lakes and slope flattenings. This paper examines the landslide hazards in the Longmenshan area caused by the earthquake using remotely sensed images, mainly Beijing-1 Microsatellite data before and after the earthquake, compared to digital elevation maps and slope gradient maps, land use and vegetation cover maps. Areas of erosion and loss of vegetation were compared from pre- and post-earthquake data, from which were calculated changes in vegetated areas, bare slopes, and mass movement during the earthquake. These events occurred over altitudes from 1000 to 4000 m and on slope angles between 25 and 55°. The results show that the total area of erosion and land movement due to the earthquake increased by 86.3 km^2 (19.2% of the study area). Compared with pre-earthquake, the areas of very low intensity soil erosion and moderate intensity soil erosion were respectively reduced by 3.6 km^2, 24.3 km^2 and 30.9 km^2. On the other hand, the areas of severe and very severe intensity soil erosion were substantially increased by 45.8 km^2 and 99.2 km^2. In the post-earthquake stage, the bare areas (vegetation cover <15%) have increased by 65.8 km^2. Without vegetation, the denuded earthquake damaged slopes and other high risk sites have become severe erosion problems. Thus, it is essential to continue long-term monitoring of mass wasting in the denuded areas and evaluate potential risk sites for future landslides and debris flows. We anticipate that these results will be helpful in decision making and policy planning for recovery and reconstruction in the earthquake-affected area.

1. Introduction

1.1. Wenchuan Earthquake

A catastrophic earthquake measuring 8.0 on the Richter scale struck Sichuan Province in southwestern China on May 12, 2008, the country's worst natural disaster in more than 30 years, with 87,419 killed or missing and 374,176 injured (Xinhua News Agency, July 21, 2008). The Wenchuan Earthquake affected 417 cities and districts of 10 autonomous prefectures and municipalities throughout Sichuan, Gansu, Shanxi, Chongqing, Yunnan Provinces, covering a total area of approximately 500,000 km^2 (Fig. 1). The core impact region of the earthquake extended from Wenchuan County to the north and east, along the three main faults in Longmenshan. The hardest hit region passed through Wenchuan, Beichuan, Mianzhu, Shifang, Qingchuan, Mao Xian, An Xian, Dujiangyan, Pingwu, and Pengzhou.

1.2. Mass wasting of soil and its effects

Earthquakes cause enormous human and economic losses, triggering cascading disasters of landslides and debris flows that adversely impact the environment (Perotto-Baldiviezo et al., 2004;

* Corresponding author. Department of Architecture & Environment, Sichuan University, Chengdu 610065, China.
E-mail address: diwubf@gmail.com (B. Di).

0034-4257/$ – see front matter © 2009 Elsevier Inc. All rights reserved.
doi:10.1016/j.rse.2009.11.011

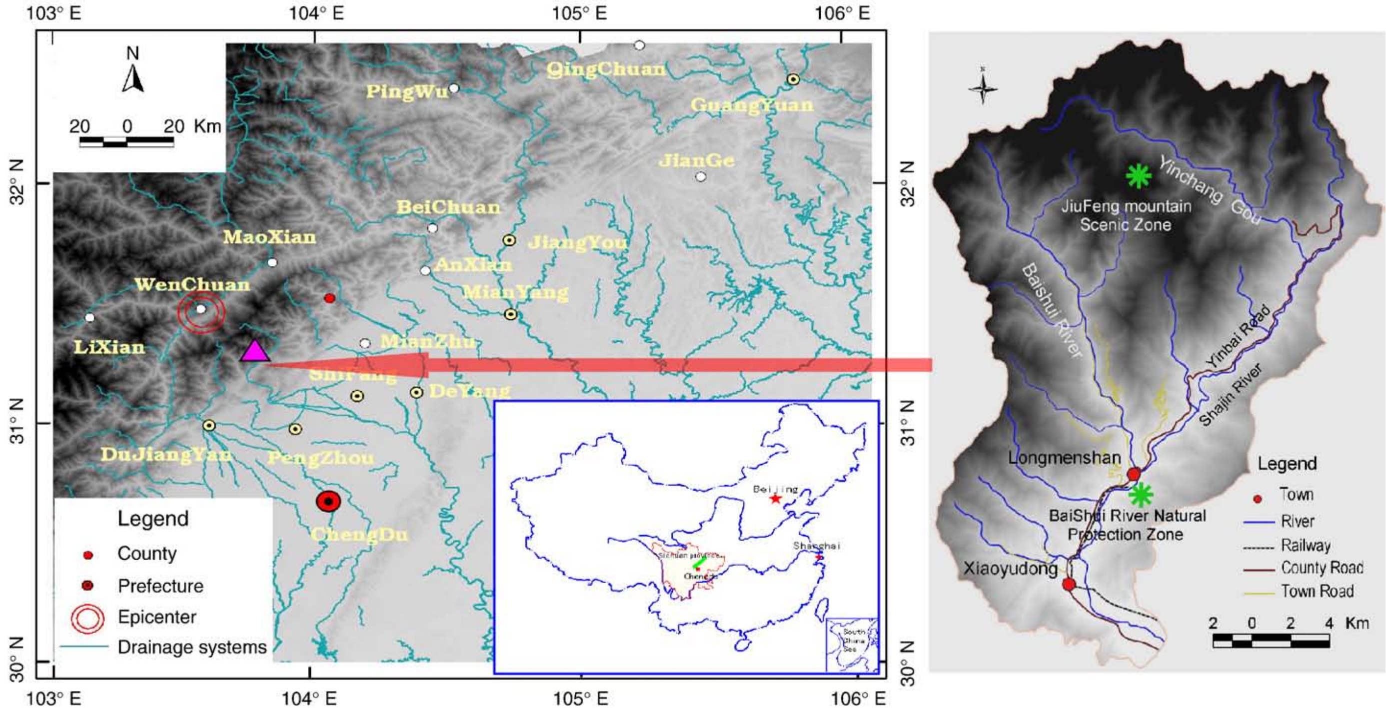

Fig. 1. Location (left) of the study area in the Longmenshan region and shaded relief map (right) with infrastructure and rivers identified in the study area.

Lin et al., 2006). The powerful Wenchuan Earthquake, the most destructive in 100 years (Xu et al., 2009) caused significant ecological and human disasters in this populated region, because of extensive soil and rock transport in avalanches, landslides, rockfalls, debris flows, granular flows, formation and release of barrier lakes, and slope flattening, all of which occurred many times following the earthquake. In China, the terms describing these forms of mass wasting and landslide processes are defined as different types of soil erosion based on the forcing agent: water erosion, wind erosion, freezing erosion, gravity erosion, glacier erosion, and mixed erosion (Yang et al., 2002). Debris avalanches, landslides, rockfalls and slope flattening are special types of gravity erosion. Debris flows, granular flows and formation of barrier lakes are special types of mixed erosion. Here, we use the encompassing term "mass wasting of soil" to generally identify any of these types of land movement.

These mass movements were unleashed by the rupture of a more than 200-kilometer long section of the Yingxiu–Beichuan fault in the Longmenshan fault zone. According to the investigation by the Soil and Water Conservation Bureau of the Ministry of Water Resources of the People's Republic of China (PRC), more than 11,000 landslides and avalanche sites were identified in the Longmenshan area. The damage to drainage infrastructure created at least 256 barrier lakes in the area, flooding and water pollution. After the earthquake, potential flooding caused by the breaching of 32 barrier lakes was one of the most serious and urgent emergency problems in the earthquake-hit area (Xu et al., 2009; Cui et al., 2009). Although there are significant differences in the magnitude of mass wasting of soil from one area to another, the extent of mass wasting and land degradation has increased throughout the earthquake region since the initial earthquake. The steep slopes of this mountainous area were substantially degraded and have become highly erodible. In addition, there was large scale damage to woodlands, forests, farmlands and grasslands by the Wenchuan Earthquake. The area of forest, grassland and wetland ecosystems was reduced by 122,136 hm^2 (Ouyang et al., 2008). As a result, the functionality of these ecosystems, in terms of loss of biological resources, soil, and water conservation has decreased. For example, 65,584 hm^2 of giant panda habitat (5.9% of total panda habitat) was lost in the earthquake (Ouyang et al., 2008). Furthermore, long-term effects of erosion on site fertility include soil loss, changes in soil texture, and nutrient loss (Tripathi & Singh, 1993; Absalom & Nomndeni, 2008).

Many researchers have concentrated on evaluating earthquake impacts using direct observation from remote sensing (RS) and mathematical methods to extract information from different parts of the electromagnetic spectrum (Hansen & Franks, 1991; David, 1994; Scira, 2001; Lin et al., 2004; Bruce et al., 2004; Koi et al., 2008; Ferah, 2008). After the Wenchuan Earthquake, most immediate studies focused on barrier lakes (Chen et al., 2008a; Tong, 2008.), general characteristics of the disaster (Huang, 2008; Xie et al., 2008), impact investigation (Fan et al., 2008; Wang et al., 2008), and disaster mitigation (Cui et al., 2008). However, there is little information about the types of mass wasting processes, the location of landscape changes, and mapping of the devastatingly scarred area requires that accurate information is available. Availability of this information is necessary for appropriate decision making. Thus, we chose the Longmenshan scenic area (LMSS) as a case study, employing RS and GIS (geographic information system) methods, to quantitatively assess changes in the mass wasting types caused by the May 12th Earthquake.

1.3. Objective of research

The objectives of this study were 1) to quantify changes in mass wasting of soil in the study area from pre-earthquake (2007) to post-earthquake (2008), and 2) to map erosion intensities. We expect that this analysis can provide a methodology for quantifying the regional scale distribution of mass wasting of soil after earthquakes.

2. Materials and methods

2.1. Study area

The Yuleishan area of Longmenshan, lies in the northwest Chengdu Plain, located between 103°40′–04°55′ eastern longitude and 30°8′–31°26′ northern latitude (Fig. 1). It is 20 km from Wenchuan, covering an area of 450 km^2. Yuleishan is a mountainous region of steep topography and intertwining channels. Elevation ranges from 870 m to 4810 m with a north–south decline. The area north of Pengzhou City, near the towns of Longmenshan and Xiaoyudong experienced the most severe earthquake damage in the greater Longmenshan area. This region is remarkably rich in biodiversity and important scenic areas, such as Yinchanggou National Geological Park, Yinchanggou 4A Grade Scenery, Baishuihe National Forest Park, and Baishuihe National Nature Reserve. For example, Class I protected animals include giant panda, golden monkey, leopard and clouded leopard, cattle ling, golden eagles, and other birds such as the Green-Tailed Rainbow Pheasant, and more than 25 Class II animals like the Red panda, monkeys, red fox, leopard cat, tufted deer and other endemic species.

Geographically, the region lies in the transition between the Tibetan Plateau and the Chengdu Plains, thus, both geology and geomorphology conditions are complex. In the LMSS, the climate is typically humid subtropical monsoon, with mild winters, hot summers, and a long frost-free period with plentiful rainfall. The annual rainfall is 1225.7 mm, with 88% occurring between May and October. The yearly average temperature and yearly average sunlight duration are 15.7 °C and 1131 h, respectively.

The main river, the Jianjiang, is more than 18 km long forming a pinnate network pattern. Much of the standing vegetation in the primary branches of the Jianjiang was completely destroyed, especially in Yinchanggou and Baishuihe (Chen et al., 2008b).

The natural vegetation is classified as subtropical evergreen broad-leaf forest. Plant biodiversity is high with more than 634 species, including several protected species like *Davidia involucrata*, *Cercidiphyllum japonicum*, and *Ginkgo biloba*.

2.2. Data sources

The data were comprised of satellite images, hard copy maps, ground observations, and data obtained from the literature (Table 1). The Beijing-1 Microsatellite data were used to compare conditions before and after the earthquake. The satellite was designed and built for the Beijing Landview Mapping Information Technology Co Ltd, by Surrey Satellite Technology Ltd. at the University of Surrey (UK). Launched in October 2005 into a 686 km Low-Earth orbit, the 166 kg Beijing-1 has a life expectancy of over five years and is the most capable low cost Earth Observation (EO) satellite to date, carrying two payloads providing high-resolution (4-m) panchromatic images alongside medium-resolution (32-m) multi-spectral images covering a 600 km swath. Beijing-1 Microsatellite provides the Chinese government and commercial users information about agriculture, water resources, environment and disaster monitoring throughout China, and is the most technologically advanced member of the Disaster Monitoring Constellation (Tong & Wei, 2007). Minimum cloud interference data from pre-earthquake (2007-09-14) and post-earthquake (2008-06-04) images (Fig. 2), were used in order to estimate changes in mass wasting processes. Hard copy 2005 maps of latest land use, relief, and district were used at a scale of 1:100,000. Detailed soil and geologic maps of the region were not available for this region in China. Ground observation data included surveys in the disaster zone to determine the extent of denudation within a few days after the earthquake. The vegetation cover class data were from visual field observations which were used to calibrate the remote sensing data and other data such as the vegetation cover in different land use types and vegetation in the denuded areas prior to the Wenchuan Earthquake. Subsequently, all data were projected (Albers) and processed using ERDAS IMAGINE9.1 and ARC/INFO9.2.

Table 1
Data used in the analysis of erosion change in LMSS area.

Items	Source of acquisition	Resolution scale
Beijing-1 Microsatellite image	Ministry of science and technology. PR.C	32 m
Land use	Institute of remote sensing applications. CAS	1:100,000
DEM	State bureau of surveying and mapping. PR.C	1:50,000
District map		1:100,000
Others	TM images, field survey, literature search	

Because of our limited field data and the complex topography, as well as frequent aftershocks, it was not possible to acquire sufficient data to statistically estimate the sediment yield caused by the earthquake over the LMSS. Therefore, this research mainly focused on the areal extent of change and the spatial distribution of mass wasting processes. Nonetheless, the sediment yields for some specific disaster locations along the Yin-bai Highway that were triggered by the earthquake were calculated.

2.3. Processing methods

A variety of RS methodologies for monitoring environmental change have been developed and evaluated over the past twenty years (Elvidge & Lunetta, 1998; Rencz, 1999; Ustin, 2004). Images from the Beijing-1 Microsatellite and Landsat Thematic Mapper (TM) are the primary data sources for the Land use and Land cover (LULC) analysis, supplemented by Landsat TM data. A schematic flow chart is presented in Fig. 3, illustrating the basic steps in the processing of the RS and GIS data. Mass wasting processes were assessed using: 1) Land use data obtained from a modified 2005 land use map was used to interpret the before and after earthquake RS images. 2) Special soil erosion types were interpreted from the RS images after the earthquake and field observation. 3) Vegetation cover was computed from a Dimidiate pixel model (Hu et al., 2007) based on the normalized difference vegetation index (NDVI), 4) Slope was obtained from a DEM (Digital Elevation Model) which was generated from the contour lines of 1:50,000 topographic digital data using the terrain analysis function in Arc/GIS (ESRI, Redlands, CA), 5) The intensity of mass wasting was estimated in IDL (Interactive Development Language) using the MWR model coupling the previous factors for each pixel, thus, computing their spatial relationships. The procedure uses the image pixel as a basic unit, identifies the spatial location of the soil erosion factors with overlay analysis and completes the estimation of mass wasting intensity from classification factors including land use, vegetation cover, and the slope gradient (MWR, 2007). While more detailed models are available, the data to run such models (e.g., sufficiently detailed soil and geologic maps) is not available for this region of China.

2.3.1. Land use

Land use and Land cover (LULC) is a significant dynamic parameter that affects the erosion process (Poesen & Hooke, 1997). The land use map was extracted from the images of the China–Brazil Earth Resources Satellite by the Institute of Remote Sensing Applications, Chinese Academy of Sciences in 2005 at a scale of 1:100,000. The 2005 digital land use map was used to train a new 2008 land cover map using pre-earthquake and post-earthquake multi-spectral images from the Beijing-1 Microsatellite. Initially, the images were rubber sheeted to match ground control locations which produced relative coordinate errors of less than a pixel. For the special soil erosion types, the spectral information for each type was found to be distinct compared to the pre-earthquake image. Thus, it was relatively easy to extract the special soil erosion types based on this difference. The land use categories consisted of arable land, irrigated farmland, woodland, grassland, constructed land, water bodies, and the areas of mass movement. To assess the accuracy of the classification, the extracted land use map was verified with the ancillary data, such as field observations and pictures from different land use types (including the denuded area) recorded with the GPS position information. Then, the

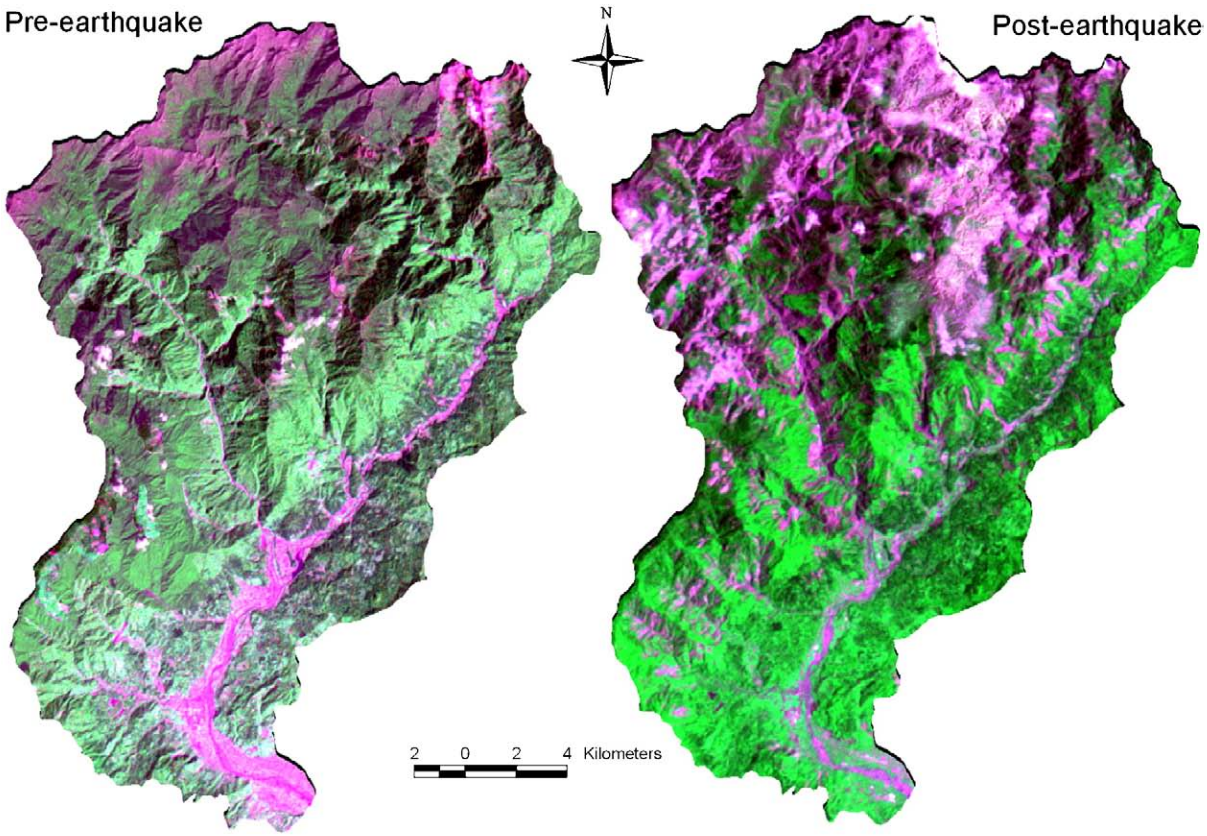

Fig. 2. The pre-earthquake and post-earthquake images from the Beijing-1 Microsatellite. Shades of green are vegetated areas and magenta are bare ground.

2005 land use map was used to extract the preexisting land cover types and the post-2008 earthquake types, which were updated using our field data from May 2008. The loss of land use classes was determined by overlaying the image based map of post-earthquake mass wasting sites over the 2005 land use map.

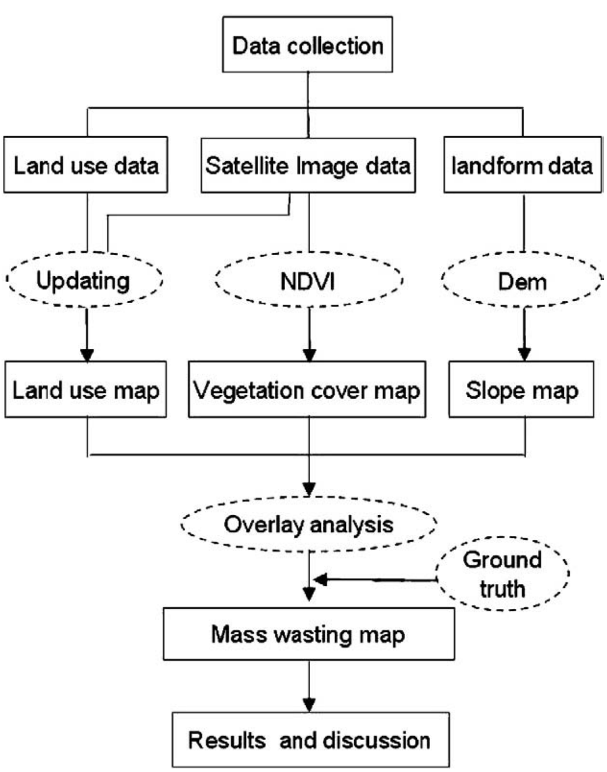

Fig. 3. Data processing flow chart.

2.3.2. Vegetation cover

Vegetation cover is the erosion risk variable that is most affected by human manipulation, and thus it is an important component of any predictive model (Sahin & Kurum, 2002; Trimble, 1990). In a holistic sense, each vegetation cover type integrates and incorporates past land use, mass wasting processes, and other environmental parameters.

NDVI is sensitive to differences in canopy greenness and biomass. It is used to rank the relative magnitude of vegetation density as well as vegetation cover. In order to acquire high precision vegetation cover data, we cross-calibrated 2007 pre-earthquake and 2008 post-earthquake Beijing-1 Microsatellite images using uniform, invariant polygons in the thematic maps, because there are no calibration parameters for Beijing-1 Microsatellite images. The calibration procedure is based on the universal equation (Chen et al., 2008c)

$$L = V_{\mathrm{gain}} V_{\mathrm{DN}} + V_{\mathrm{offset}} \quad (1)$$

where L is the surface radiation; V_{gain} is the sensor's gain parameter; V_{DN} is the measured pixel value in the respective remote sensing image; and V_{offset} is the sensor's compensation parameter.

First, the Beijing-1 Microsatellite data was matched to the projection and resolution of the Landsat TM images; the root mean square error was kept within 0.5 pixels. We randomly selected 4000 corresponding pixels in each image. Afterwards, a regression was created between the Digital Number of selected pixels and the calibration equations for the Near-Infrared (NIR) band and RED band of Beijing-1 Microsatellite, as follows:

$$\text{For pre}-\text{earthquake}: \text{NIR}: L = 0.7313{*}DN + 28.89 \quad R^2 = 0.5548 \quad (2)$$

$$\text{RED}: L = 1.3317{*}DN + 12.577 \quad R^2 = 0.6693 \tag{3}$$

$$\text{For post-earthquake}: \quad \text{NIR}: L = 1.6598{*}DN + 0.7457 \quad R^2 = 0.5986 \tag{4}$$

$$\text{RED}: L = 4.6819{*}DN + 15.832 \quad R^2 = 0.6844 \tag{5}$$

Subsequently, NDVI was calculated in pre- and post-earthquake images with the cross-calibrated NIR and RED bands of Beijing-1 Microsatellite based on Eq. (6) (Justice et al., 1985). Consequently, the vegetation cover was estimated based on Eq. (7).

$$NDVI = \frac{NIR - RED}{NIR + RED}. \tag{6}$$

$$f = \frac{NDVI - NDVI_s}{NDVI_v - NDVI_s} \tag{7}$$

where f is the vegetation cover; $NDVI_V$ is the NDVI of fully vegetation cover; and $NDVI_S$ is the NDVI of bare soil land cover (denuded area).

In this study, the land use map and field observation data were compared and used to select 20 forest areas of best growth, taking the average NDVI of the best growth as $NDVI_V$; and similarly selected 20 denuded lands where the soil or rock were exposed, and used the average NDVI as $NDVI_S$. Afterward, the vegetation cover was calculated and calibrated using the field measurements, which included 23 samples from 5 land use types that were located along the Yin-bai Highway and identified by visual inspection (Table 2). The comparison shows that the precision in the vegetation cover estimate is about 87.0%. Subsequently, six different classes of vegetation cover were extracted from the vegetation cover map and used in this study (Table 3).

2.3.3. Slope

The slope gradient, characterizes the rate of elevation change in the direction of steepest descent, which affects the velocity of both surface and subsurface flow, and hence erosion potential. As the slope angle increases, shear stress in soil or other unconsolidated material generally increases as well (Lee et al., 2004). The slope gradient was calculated from the DEM. The GIS was used to generate a gradient classification map with the following classes: <5°, 5–8°, 8–15°, 15–25°, 25–35°, >35° (MWR, 2007; Tian et al., 2009).

Table 3
The classification of vegetation cover.

Class	Vegetation cover(%)
1	>75
2	60–75
3	45–60
4	30–45
5	15–30
6	<15

2.4. Evaluation criteria of mass wasting of soil

The analysis of mass wasting intensity distribution is based on an expert knowledge method which connects spatial information with the main soil erosion factors, including land use, vegetation cover, and slope gradient. Expert knowledge was derived from the SL190-96 Standards for Classification and Gradation of Soil Erosion of the PRC, which was established in 1997 and revised in 2007 (MWR, 2007). The SL190-96 Standards were successfully used to monitor soil erosion at national and regional scales in China (Zhao et al., 2002; Chen et al., 2005). In the MWR standard, a set of knowledge-based rules, for assessing soil erosion in this heterogeneous hilly catchment were defined by multi-disciplinary resource-experts with knowledge of the local catchment resources, in addition to the field observations. Soil erosion intensity was divided into six grades (non-erosion, very low, low, moderate, severe and very severe.) by the affecting factors and the input parameters required by the model, which are easily produced by GIS and RS techniques. Different grades of soil erosion are clarified by the annual average soil erosion modulus defined from long-term field observations, which are <500 t/km^2 (non-erosion), 500–2500 t/km^2 (very low), 2500–5000 t/km^2 (low), 5000–8000 t/km^2 (moderate), 8000–15,000 t/km^2 (severe), >15,000 t/km^2 (very severe), respectively. Additionally, the special soil erosion types (avalanches, landslides, rockfalls, debris flows, granular flows, and slope flattenings) and collapsed buildings triggered by the earthquake are considered to be a severe erosion class. Based on these premises, a

Table 2
Comparison between predicted vegetation cover class from RS images and field observations by visual inspection.

Order no.	Longitude (°)	Latitude (°)	Land use type	Vegetation cover class		Remark
				Simulated	Field measurements	
1	103.7605	31.2225	Constructed land	1	1	
2	103.7822	31.2247	Arable land	3	3	
3	103.7908	31.2376	Water bodies	1	1	
4	103.8001	31.2514	Arable land	2	2	
5	103.7993	31.2555	Constructed land	2	1	
6	103.7841	31.2559	Constructed land	1	1	Landslide
7	103.8047	31.2572	Arable land	3	3	
8	103.8197	31.2643	Water bodies	1	1	
9	103.8091	31.2671	Arable land	3	3	
10	103.8193	31.2687	Arable land	3	3	
11	103.8259	31.2723	Arable land	3	3	
12	103.8263	31.2851	Arable land	2	3	
13	103.8377	31.2932	Woodland	4	4	
14	103.8476	31.2948	Woodland	1	1	Barrier lake
15	103.8660	31.3019	Woodland	4	4	
16	103.8671	31.3076	Woodland	2	2	
17	103.8682	31.3132	Woodland	3	3	
18	103.8743	31.3201	Arable land	3	3	
19	103.8646	31.3219	Woodland	5	5	
20	103.8738	31.3262	Constructed land	1	1	
21	103.8730	31.3326	Woodland	3	2	
22	103.8641	31.3348	Grassland	1	1	Avalanche
23	103.8801	31.3471	Woodland	1	1	Landslide

Table 4
Classification criteria of mass wasting intensity.

Land use type	Vegetation cover rate(%)	Slope gradient (degrees)				
		5–8	8–15	15–25	25–35	>35
Woodland	60–75	VL	VL	VL	L	L
Grassland	45–60	VL	VL	L	L	M
	30–45	VL	L	L	M	S
	<30	L	L	M	S	VS
Arable land		VL	L	M	S	VS
Irrigated farmland, construction land, water body		N	N	N	N	N
Special soil erosion		VS	VS	VS	VS	VS
Collapsed buildings		<20%	20–40%	40–60%	60–80%	>80%
		VL	L	M	S	VS

Mass wasting intensity: N, non-erosion; VL, very low; L, low; M, moderate; S, severe; VS, very severe.

conceptual model used to estimate soil erosion intensity is defined as the following:

$$E = f(L, S, C, SP) \tag{8}$$

where E is the soil erosion intensity, L the land use type, S the slope, C the vegetation cover, and SP the special erosion types.

In general, a change can be determined from the E value. The soil erosion intensity classification criteria listed in Table 4 was used to qualitatively determine six categories of soil erosion intensity.

3. Results

Using the classification criteria in Table 4, the GIS overlay analysis of vegetation cover, land use and slope gradient maps for pre- and post-earthquake was used to determine the mass wasting maps for pre- and post-earthquake that are presented in Fig. 4.

Total area of soil erosion before the earthquake was 302.98 km^2, accounting for 67.3% of the study area. As seen in Table 5, the non-movement zone, comprising the largest proportional area, accounts for 32.7% of the study area, the very low intensity zone accounts for 6.7%, the low intensity zone accounts for 25.3%, the moderate intensity zone accounts for 21.8%, the severe intensity zone accounts for 7.5%, and the very severe intensity zone accounts for 6.1%.

After the earthquake, the total area of mass wasting increased by 28.5% to 389.28 km^2, which accounts for 86.5% of the study area. As seen in Table 5, the non-mass wasting zone accounted for only 13.5%, the very low intensity zone accounted for 5.9%, the low intensity zone accounted for 19.9%, the moderate intensity zone accounted for 14.9%, the severe intensity zone accounted for 17.7%, and the very severe intensity zone, with the second largest area, accounted for 28.1%.

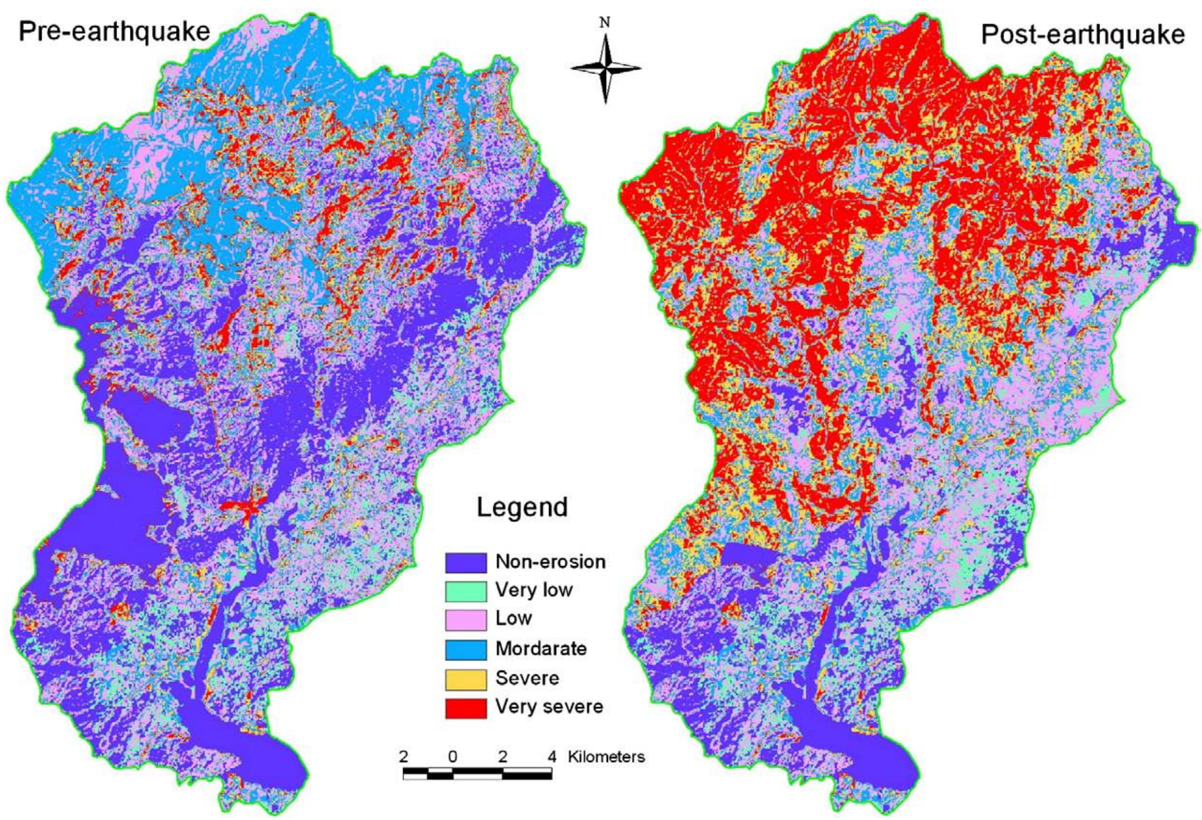

Fig. 4. Mass wasting maps of pre- and post-earthquake in the Longmenshan area. Colors indicate soil erosion classes.

Table 5
Comparison of mass wasting area (km^2) between 2007 and 2008.

Item	Non-erosion		Very low		Low		Moderate		Severe		Very severe	
	Area	%	Area	%	Area	%	Area	%	Area	%	Area	%
2007	147.02	32.67	30.08	6.68	113.80	25.29	98.00	21.78	33.88	7.53	27.22	6.05
2008	60.72	13.49	26.45	5.88	89.53	19.90	67.12	14.91	79.72	17.71	126.46	28.10
Change	86.30	19.18	3.63	0.80	24.26	5.39	30.88	6.87	−45.84	−10.18	−99.24	−22.05

Table 6
Conversion matrix of mass wasting area (km^2) of different mass wasting intensities.

Item	2008						Total (2007)
	Non-erosion	Very low	Low	Moderate	Severe	Very severe	
2007							
Non-erosion	53.62	4.28	23.69	18.59	21.15	25.69	147.02
Very low	1.86	19.28	7.83	1.12	0.00	0.00	30.08
Low	3.30	2.75	49.86	20.15	23.17	14.57	113.80
Moderate	0.84	0.14	5.48	19.72	15.69	56.13	98.00
Severe	0.34	0.00	2.20	4.94	13.84	12.56	33.88
Very severe	0.77	0.00	0.48	2.60	5.86	17.51	27.22
Total (2008)	60.72	26.45	89.53	67.12	79.72	126.46	450.00

The mass wasting results are presented in Table 5. Compared with pre-earthquake, the total area of mass wasting in the post-earthquake period sharply increased from 302.98 km^2 to 389.28 km^2, an increase of 86.30 km^2 (accounting for 19.2% of the study area). For different movement intensities, the very low erosion, low erosion, and moderate erosion aerial extents were all respectively reduced by 3.63 km^2, 24.26 km^2 and 30.88 km^2. In contrast, the areas of severe and very severe mass wasting substantially increased by 45.84 km^2 and 99.24 km^2. Obviously, the area of mass wasting changed in two ways: the area of strong mass wasting increased, while the area of weak mass movement decreased. For instance, a non-erosion pre-quake area of 46.84 km^2 changed into severe and very severe post-earthquake levels, respectively to 21.15 and 25.69 km^2 (Table 6). On the whole, Table 5 demonstrates that tremendous changes took place in the non-mass wasting, severe and very severe mass wasting categories.

4. Discussion

4.1. Spatial characteristics of mass wasting changes

In general, distribution of earthquake-triggered landslides is most strongly influenced by slope steepness, geology and shaking intensity (Wang et al., 2007). Accordingly, we observed that a combination of elevations and slopes may have contributed most frequently to the distribution of mass wasting triggered by the Wenchuan Earthquake. A statistical analysis of soil erosion distributions was conducted for the landslides that were concentrated in the study area.

Five elevation ranges were defined to investigate mass wasting intensity: <1000 m, 1000–2000 m, 2000–3000 m, 3000–4000 m and >4000 m. Some changes with elevation were revealed from GIS overlays (Fig. 5). For severe and very severe erosion, the area of movement increased in all elevation ranges, and these increases were corroborated by calculating changes between 1000 m and 4000 m. For moderate erosion, clear changes were seen between 3000 and 4000 m, with minimal change at elevations below 3000 m. For low soil erosion, a detectable decrease was seen in this class between 2000 and 4000 m. There was insignificant change in the very low erosion area. Compared with pre-earthquake for the non-erosion area, the post-earthquake area decreased at all elevation ranges with the biggest change occurring between 1000 m and 4000 m. Summarizing all of these changes, we concluded that the greatest change in soil

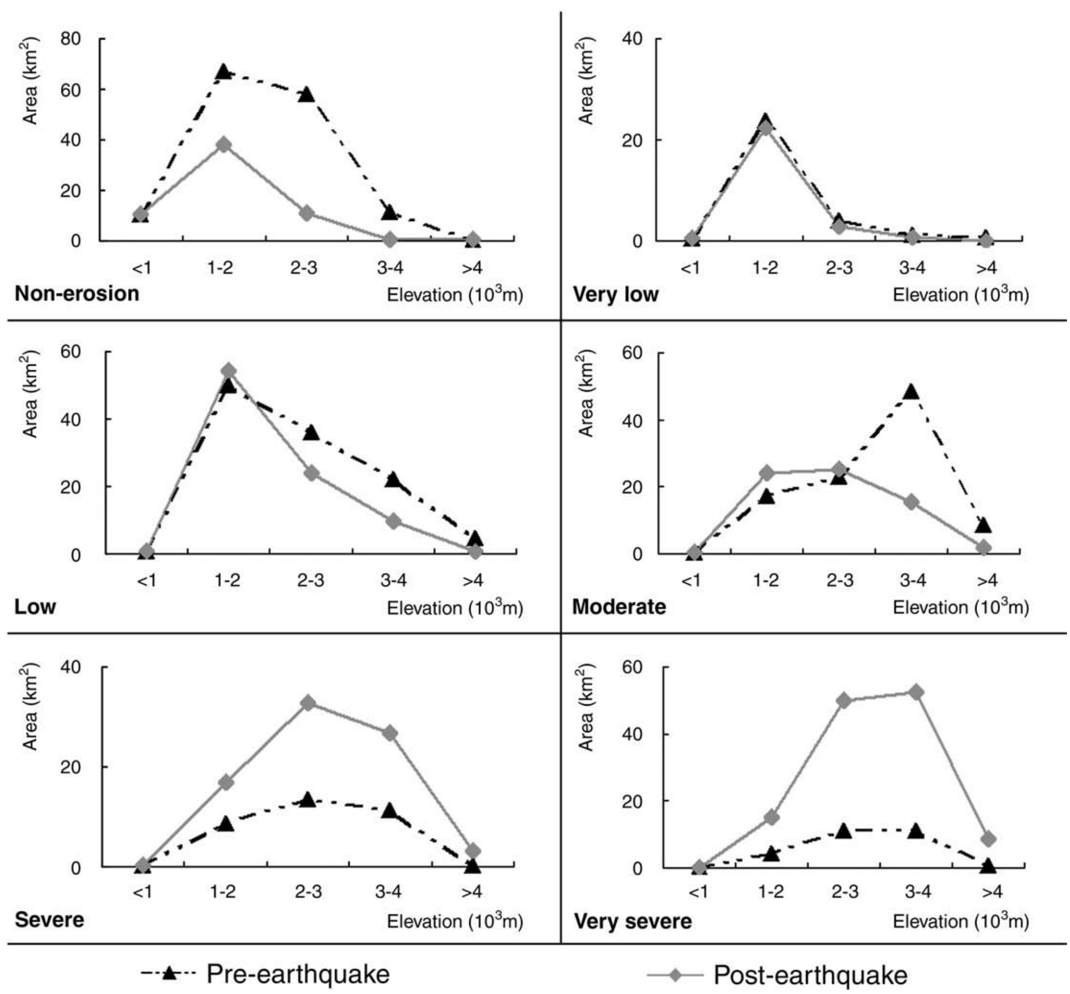

Fig. 5. Changes in the area of mass wasting classes in different elevation zones.

erosion occurred between 1000 m and 4000 m, while negligible change occurred below 1000 m and above 4000 m.

Following the earthquake, the eight soil erosion intensity slope range parameters revealed some changes (Fig. 6). The areas for severe and very severe erosion increased sharply in zones with slopes from 25° to 55°. For moderate erosion, there was a clear increase between 8° and 35°, while there was a remarked decrease for slopes between 35°and 55°. For low erosion classes, a decrease was distinguishable between 25° and 55°. There was inconspicuous change in the lowest erosion levels. The area of the non-erosion class decreased, compared with pre-earthquake, with the biggest change occurring in slopes between 25° and 55°. We concluded that the greatest changes in soil erosion were seen in slopes between 25° and 55°, while negligible changes were evident at slopes below 8 °and above 55°.

4.2. Mass wasting of soil change driving forces

The area of mass wasting increased dramatically in the study area from pre- to post-earthquake as illustrated in the LMSS maps (Figs. 2, 4 and 7). Thus, areas which pre-earthquake exhibited no erosion became classified as areas of high erosion. The driving force for these changes is mainly the consequences of the special mass wasting soil types. The bare areas (vegetation cover <15%) in pre- and post-earthquake shown in Fig. 7, show that the previous denuded area was 17.46 km^2 but increases to 83.26 km^2 after the earthquake. The denuded area increased 65.81 km^2, mostly attributed to the Wenchuan Earthquake.

From field surveys, it was possible to ascertain that denuded sites were widely distributed throughout the study area. We estimated that more than 7% of the ecosystem area consisting of forest, shrub, meadow, river and farmland land cover types were destroyed by the earthquake. Especially in the northern region of the LMSS, the fraction of degraded area reached 30% to 40% in some parts of the core impact region (Fig. 8).

Numerous special soil erosion types were triggered by the earthquake. However, due to the complex topography and inaccessible conditions, as well as frequent aftershocks, a complete and accurate survey of the special soil erosion type disasters over the full region was not possible. A few of the denuded sites, however, were accessible and surveyed along the Yin-bai Highway. For small denuded sites, the length, width and average thickness of the mass moved can be directly estimated in the field. Otherwise, for large denuded sites, we can extract the area of mass movement from the Beijing-1 Microsatellite images and estimate the average thickness from the field survey. Then, for these sites, the volume of soil movement can be calculated from these parameters. There were 59 denuded sites accessible from the highway for which field measurements found 5540×10^4 m^3 of transported sediment. As shown in Table 7, there were 22 sites with landslides, which comprised the greatest sediment yield, accounting for 52.2% of the total. Avalanches occurred at 15 sites (28.5% of the sediment yield), slope flattening at 5 sites (16.7%) and debris flows at 17 sites (2.6%). For the Jiufengshan landslide (No.7 in Fig. 9), more than 350×10^4 m^3 of sediment was released.

Unstable sites of soil erosion were mainly located at slope toes along the Yin-bai Highway and denuded soils and rocks wedged in river valleys or piled on hillslopes along the highway. Analysis of some typical high risk sites (Table 8) showed that they triggered extensive

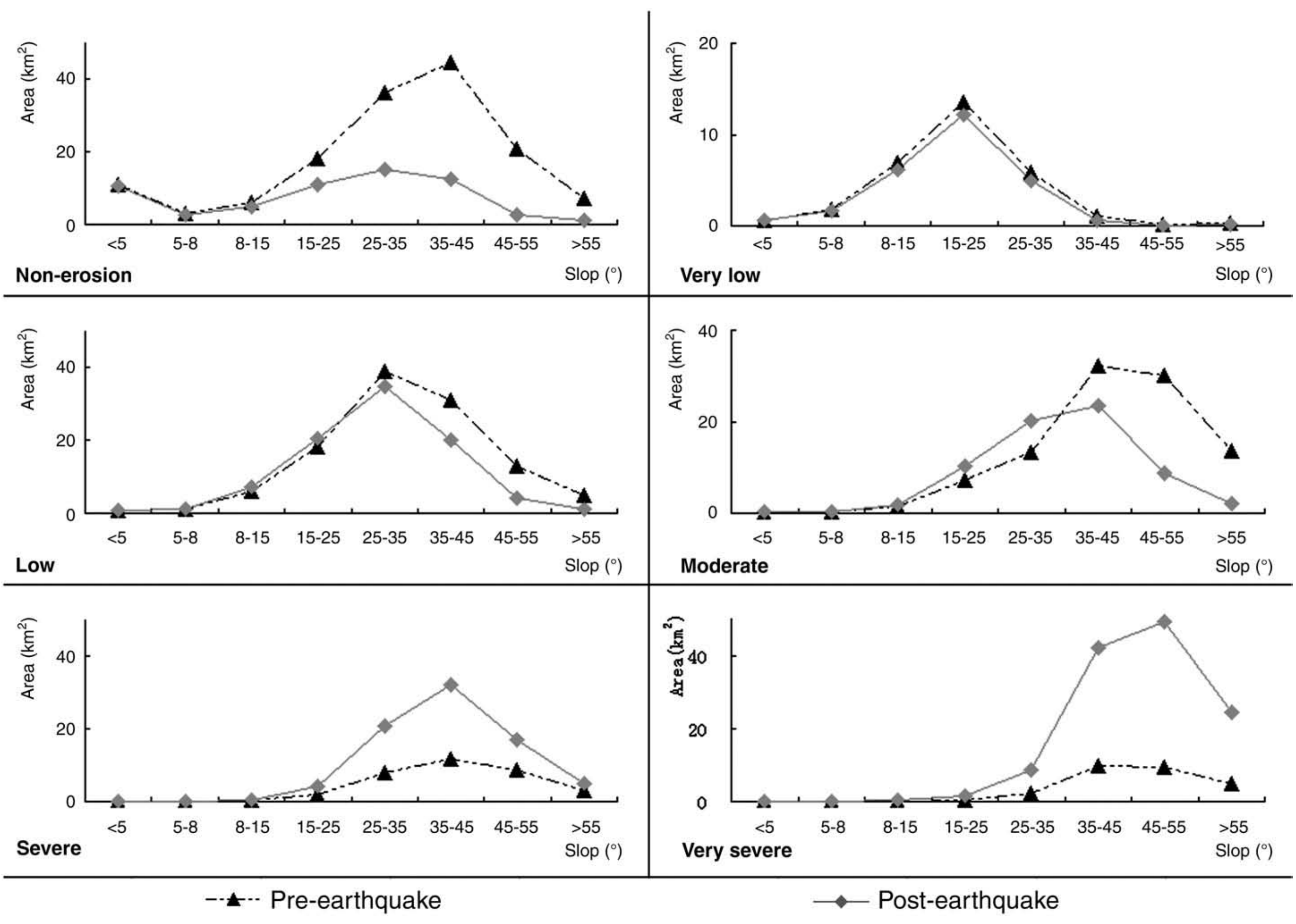

Fig. 6. Changes in the area of mass wasting classes in different slope ranges.

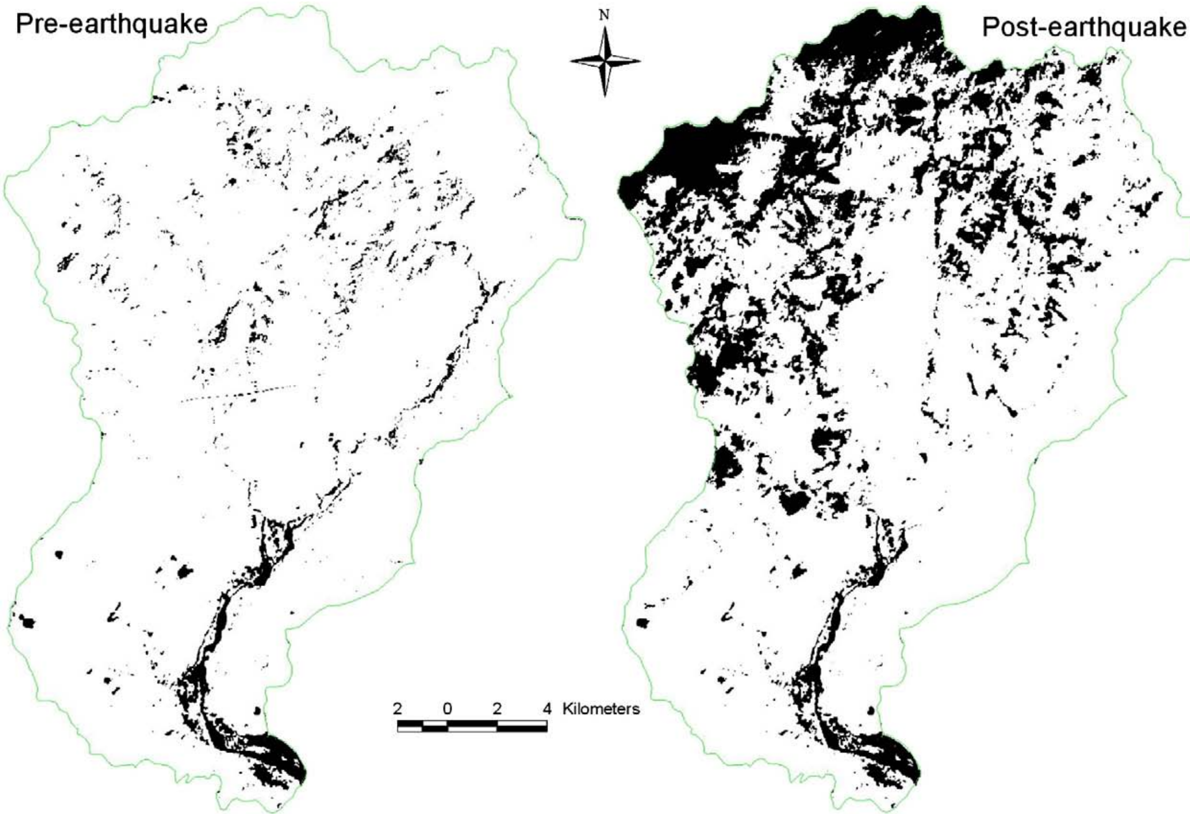

Fig. 7. Bare area (vegetation cover <15%) maps of pre- and post-earthquake Longmenshan area.

and cascading mass wasting problems. The Wenchuan Earthquake dramatically altered the natural geology and landforms across most of the LMSS. Many rock and soil avalanches, landslides, and giant debris flows were deposited in steep-sloped valley and gully areas which increase the potential for mass wasting to continue in the down-slope direction. The earthquake, released a large mass of soil and rock material into the river beds joined to the steep slopes that serve as energy sources for eruption of new debris flows, which will continue to occur for several years after this earthquake.

For example, steep slopes along the Shajin River have accumulated huge amounts of material in the stream branches that substantially increase mass and energy sources for eruption of new debris flows. After the earthquake, there were five reported debris flow events triggered by monsoon storms in the study area between June and September in 2008. Some of these debris flow events demolished houses, damaged the Yinbai Highway, blocked traffic, buried farmland, and further endangered human life and property. Our investigation in Yinchanggou, showed that several debris flows, combined with landslides and a flood, occurred on the night of July 14, 2008. The deposits contained a large amount of soil and rock mass that blocked eight roads and damaged several buildings. Similar debris flows and landslides occurred in this area in summer 2009. It is clear from these anecdotes that there is considerable increased and continuing risk of debris flows, especially during the rainy monsoon season. Considering current conditions, it is likely that

Fig. 8. Landslides and avalanches induced by the 2008 earthquake in the valley of the Shajin River (Left) and Yinchang Gou gully (Right). Both areas had mature forest vegetation before the Wenchuan Earthquake. The vegetation was previously distributed over the lower hillslopes, crest lines, and along the downslopes.

Table 7
The number and sediment of mass wasting sites on Yin-bai Roadsides.

	Landslide	Avalanche	Slope flattening	Debris flow	Total
Number	22	15	5	17	59
Sediment (10^4 m^3)	2892.05	1576.80	925.00	143.40	5537.25

continued landslides and debris flows will be the major types of mass wasting in Longmenshan. Therefore, mitigation of debris flow and landslide occurrence by natural restoration and managed reconstruction is definitely needed.

5. Conclusion

To understand the dynamics of mass wasting over time and space, better understanding of the changes in the earthquake-affected area is necessary. Quantitative estimates of mass wasting of soil have been lacking in the Longmenshan area after the May 12th earthquake, because there little detailed data are available. However, because the rapid erosion processes are still underway it is important to begin to build such understanding to prevent future disasters of this magnitude. The Beijing-1 Microsatellite can observe locations of mass movement continuously for 24 h thus providing high temporal and high spatial resolution digital imagery that is needed for effective disaster

Fig. 9. Jiufengshan landslide occurring in July 2009 is one of the largest landslides in the LMSS. It is estimated that the upper sliding body collided forcefully and induced more mass movements as it fell from the upper steep slopes. This landslide entirely buried the Number 7 village and caused almost 70 deaths. The resulting 15° deposit slope also obstructed the main river channel.

Table 8
Features of special erosion sites on Yin-bai Roadsides.

Type	Order no.	Longitude (°)	Latitude (°)	Sediment (10^4 m^3)	Description
Landslide	1	103.5015	31.1703	140	Threatened highway with an extent of 200 m.
	2	103.5156	31.1834	140	Threatened highway with an extent of 300 m.
	3	103.4931	31.1706	150	Destroyed highway.
	4	103.4917	31.0000	220	Threatened highway with an extent of 200 m.
	5	103.5051	31.1754	200	Destroyed highway
	6	103.4815	31.1621	300	Clogged river. Threatened villages.
	7	103.5049	31.1728	350	The deposit slope was 15°. Barred river.
Avalanche	1	103.5240	31.1944	50	Threatened highway
	2	103.5356	31.2046	72	Threatened highway and river.
	3	103.4612	31.1328	600	Destroyed highway
	4	103.4524	31.1100	750	Destroyed highway
Slope flattening	1	103.4645	31.1358	60	Threatened highway and villages
	2	103.4601	31.1033	360	Threatened highway and villages
	3	103.4649	31.1457	500	Destroyed highway and market town
Debris flows	1	103.4941	31.1611	38	Threatened 100 people's safety
	2	103.4920	31.1549	22	Threatened 35 people's safety

monitoring and response. Using RS and GIS techniques as the primary methods, we estimated mass wasting processes by effectively coupling expert knowledge and data on the factors that influence soil erosion.

Enormous regional changes were induced mostly by the special soil erosion types (avalanches, landslides, rockfalls, debris flows, granular flows and slope flattening) and collapsed buildings triggered by the earthquake. The greatest soil erosion occurred between 1000 m and 4000 m elevation and on slopes between 25° and 55°, while negligible change occurred at elevations below 1000 m and above 4000 m and on slopes below 8°and above 55°. Compared to the pre-earthquake condition, the total area of soil erosion increased by 86.30 km^2 (19.2% of the study area). Areas of non-erosion experienced the greatest areal reduction, while the severe and very severe erosion classes exhibited the greatest areal increases.

Without vegetation cover, the topsoil and sediment in the earthquake denuded areas and other high risk areas will continue to be unstable in the coming years. During the rainy season, large quantities of sediment are transported into rivers from these areas. Consequently, there is continuing need to monitor the high risk and potential risk mountain sites for soil erosion hazards.

Acknowledgements

This work was supported by National "973" Project (2008CB425803), Mountain Hazard & the Earth's Surface Processes Key laboratory, CAS (LF08006), the National Key Technologies R&D project "Ecological protection and technology demonstration of debris flow and landslide prevention for large hydropower project area in South-West China" (No. 2006BAC10B04) and 111 Project (No. B08037). The satellite images were provided by Beijing Landview Mapping Information Technology Co. Ltd. The authors gratefully acknowledge to Dr. Zhiguang Li, Professor Peng Cui for their help and direction. What's more, we also appreciate Chen Ye, Heather Sturman, Fabio, Professor Earl Bossard and Professor Carla Bossard for help in revisions.

References

Absalom, M. M., & Nomndeni, N. (2008). Mapping of soil erosion using remotely sensed data in Zombodze South, Swaziland. *Physics and Chemistry of the Earth*, *33*, 800−806.

Bruce, D. M., Donald, L. T., Fausto, G., & Paola, R. (2004). Landslides, earthquakes, and erosion. *Earth and Planetary Science Letters*, *229*, 45−59.

Chen, X. Q., Cui, P., Cheng, Z. L., You, Y., Zhang, X. G., He, S. M., & Dang, C. (2008a). Emergency risk assessment of dammed lakes caused by the Wenchuan Earthquake on May 12, 2008.*Earth Science Frontiers*, *15*, 244−249 China.

Chen, N. S., Di, B. F., Li, Z. L., & Li, H. (2008b). The features and measures of mountain hazards triggered by earthquake in Longmenshan Mountains.*Journal of Mountain Science*, *26*, 272−275 China.

Chen, Z. C., Liu, X., Li, J. S., Luo, W. F., Zhang, J., Zhang, J., Zhang, X., & Zhang, B. (2008c). The cross calibration of Beijing-1 Microsatellite multispectral sensors.*Journal of Astronautical*, *29*, 637−643 China.

Chen, W. H., Liu, L. Y, Zhang, C., Pan, Y. C., Wang, J. H., & Wang, J. D. (2005). The fast method of soil erosion investigation based on remote sensing. *Research in Soil and Water Conservation*, *12*, 8−10.

Cui, P., Zhu, Y. Y., Han, Y. S., Chen, X. Q., & Zhuang, J. Q. (2009). The 12 May Wenchuan earthquake-induced landslide lakes: Distribution and preliminary risk evaluation. *Landslides*, *6*, 209−223.

Cui, P., Wei, F. Q., He, S. M., You, Y., Chen, X. Q., Li, Z. L., Dang, C., & Yang, C. L. (2008). Mountain disasters induced by the earthquake of May 12 in Wenchuan and the disasters mitigation.*Journal of Mountain Science*, *26*, 280−282 China.

David, K. K. (1994). The importance of earthquake-induced landslides to long-term slope erosion and slope-failure hazards in seismically active regions. *Geomorphology*, *10*, 265−284.

Elvidge, C. D., & Lunetta, R. (Eds.). (1998). *Remote sensing change detection: Environmental monitoring applications and methods* MI: Ann Arbor Press.

Fan, J. R., Tian, B. W., Cheng, G. W., Tao, H. P., Zhang, J. Q., Yan, D., Su, F. H., & Liu, B. T. (2008). Investigation on damming object induced by the earthquake of Wenchuan on May 12 based on multi-platform remote sensing.*Journal of Mountain Science*, *26*, 257−262 China.

Ferah, Akinci (2008). The aftermath of disaster in urban areas: An evaluation of the 1999 earthquake in Turkey. G.U. *Journal of Science*, *21*(2), 43−49.

Hansen, A., & Franks, C. A. M. (1991). Characterisation and mapping of earthquake triggered landslides for seismic zonation. *Proc.4th Int. Conf. on Seismic Zonation, Stanford, California*, *1* (pp. 149−195).

Huang, R. Q. (2008). Characteristics of geological disasters of 5·12 Wenchuan Earthquake and recommendation on its impact on reconstruction.*Chinese Geological Education*, *2*, 21−24 China.

Hu, Z. Q., He, F. Q., Yin, J. Z., Lu, X., Tang, S. L., Wang, L. L., & Li, X. J. (2007). Estimation of fractional vegetation cover based on digital camera survey data and a remote sensing model. *Journal of China University of Mining and Technology*, *17*, 116−120.

Justice, C. O., Townshend, J. R. G., Holben, B. N., & Tucker, C. J. (1985). Analysis of the phenology of global vegetation using meteorological satellite data. *International Journal of Remote Sensing*, *6*, 1271−1318.

Koi, T., Hotta, N., Ishigaki, I., & Matuzaki, N. (2008). Prolonged impact of earthquake-induced landslides on sediment yield in a mountain watershed: The Tanzawa region, Japan. *Geomorphology*, *101*, 692−702.

Lee, S., Choi, J., & Min, K. (2004). Probabilistic landslide hazard mapping using GIS and remote sensing data at Boun, Korea. *International Journal of Remote Sensing*, *25*(11), 2037−2052.

Lin, C. Y., Lo, H. M., Chou, W. C., & Lin, W. T. (2004). Vegetation recovery assessment at the Jou-Jou Mountain landslide area caused by the 921 Earthquake in central Taiwan. *Ecological Modelling*, *176*, 75−81.

Lin, W. T., Lin, C. Y., & Chou, W. C. (2006). Assessment of vegetation recovery and soil erosion at landslides caused by a catastrophic earthquake: A case study in Central Taiwan. *Ecological Engineering*, *28*, 79−89.

MWR (Ministry of Water Resources, PRC) (2007). *National professional standards for classification and gradation of soil erosion (SL190-2007)* (pp. 10−15). Beijing: China Hydraulic and Hydropower Press.

Ouyang, Z. Y., Xu, W. H., Wang, X. Z., Wang, W. J., Dong, R. C., Zheng, H., Li, D. H., Li, Z. Q., Zhang, H. F., & Zhuang, C. W. (2008). Impact assessment of Wenchuan Earthquake on ecosystems. *ACTA ECOLOGICA SIN ICA*, *28*(12), 5801−5809.

Perotto-Baldiviezo, H. L., Thurow, T. L., Smith, C. T., Fisher, R. F., & Wu, X. B. (2004). GIS-based spatial analysis and modeling for landslide hazard assessment in steep lands, southern Honduras. *Agriculture Ecosystems & Environment*, *103*, 165−176.

Poesen, J. W. A., & Hooke, J. M. (1997). Erosion, flooding and channel management in Mediterranean environments of southern Europe. *Progress in Physical Geography*, *21*, 157−199.

Rencz, A. (Ed.). (1999). *Remote sensing for the Earth sciences, 3rd Edition Manual of remote sensing*, *Vol. 3*. (pp.) New York: John Wiley and Sons.

Scira, Menoni (2001). Chains of damages and failures in a metropolitan environment: Some observations on the Kobe earthquake in 1995. *Journal of Hazardous Materials*, *86*, 101−119.

Sahin, S., & Kurum, E. (2002). Erosion risk analysis by GIS in environmental impact assessments: A case study—Seyhan Köprü Dam construction. *Journal of Environmental Management*, *66*, 239−247.

Tian, Y. C., Zhou, Y. M., Wu, B. F., & Zhou, W. F. (2009). Risk assessment of water soil erosion in upper basin of Miyun Reservoir, Beijing, China. *Environmental Geology*, *57*, 937−942.

Tong, L. Q. (2008). Emergency remote sensing investigation of barrier lakes at the quake center area caused by"5·12" Wenchuan strong earthquake.*Remote sensing for Land & Resources*, *3*, 71-64 China.

Tong, Q. X., & Wei, Z. (2007). Beijing-1 Microsatellite and its data application.*Spacecraft Engineering*, *16*(2), 1−5 China.

Tripathi, R. P., & Singh, H. P. (1993). *Soil erosion and conservation* India. New Delhi: Wiley Eastern Limited pp. 305.

Trimble, W. S. (1990). Geomorphic effects of vegetation cover and management: Some time and space considerations in predicting of erosion and sediment yield. In J. B. Thornes (Ed.), *Vegetation and erosion* UK: John Wiley and Sons Ltd.

Ustin, S. L. (Ed.). (2004). *Remote sensing for natural resource management and environmental monitoring. ASPRSManual of remote sensing*, *Vol. 4*. (pp.) New York: John Wiley and Sons 736p. +cd.

Wang, W. J., Pan, Y. Z., Xu, W. H., Wang, J. J., & Bai, X. (2008). Analysis on ecosystem destroy and its ecological impact caused by earthquake in Wenchuan, Sichuan Province.*Research of Environmental Sciences*, *21*, 110−116 China.

Wang, H. B., Sassa, K., & Xu, W. Y (2007). Analysis of a spatial distribution of landslides triggered by the Chuetsu earthquakes of Niigata Prefecture. *Japan Natural Hazards*, *41*, 43−60.

Xie, H., Wang, S. G., & Kong, J. M. (2008). Distribution and characteristics of mountain hazards induced by the earthquake of May 12 in Wenchuan.*Journal of Mountain Science*, *26*, 396−401 China.

Xu, Q., Fan, X. M., Huang, R. Q., & Cee, V. W. (2009). Landslide dams triggered by the Wenchuan Earthquake, Sichuan Province, south west China. *Bulletin of Engineering and Geological Environment*, *68*, 373−386.

Yang, A. M., Wang, H., Tang, K. W., & Sun, G. (2002). Soil erosion characteristics and control measures in China. *Proceedings of 12th International Soil, Conservation Organization Conference, May 26–31, Beijing, China*, *1*, 463−469.

Zhao, X. L., Zhang, Z. X., Liu, B., & Wang, C. Y. (2002). Method of monitoring soil erosion dynamic based on remote sensing and GIS. *Bulletin of Soil and Water Conservation*, *22*, 29−32.